Influence of the preparation method on the activity of ceria zirconia mixed oxides for naphthalene total oxidation

David R. Sellick[a], Asunción Aranda[b], Tomas García[b], José M. López[b], Benjamín Solsona[c], Ana M. Mastral[b], David J. Morgan[a], Albert F. Carley[a], Stuart H. Taylor[a,*]

[a] Cardiff Catalysis Institute, School of Chemistry, Cardiff University, Main Building, Park Place, Cardiff, CF10 3AT, UK
[b] Instituto de Carboquímica (CSIC), C/Miguel Luesma, 50018 Zaragoza, Spain
[c] Departament d'Enginyeria Química, Universitat de València, C/Dr. Moliner 50, 46100 Burjassot, Valencia, Spain

ABSTRACT

Cerium/zirconium mixed oxides, with different Ce/Zr ratios, have been synthesised by a co-precipitation method using two different precipitating agents (sodium carbonate and urea) and tested for the total oxidation of naphthalene. Catalysts were characterised by N_2 adsorption, XRD, Raman, TPR, XPS and DRIFTS. Ceria prepared by carbonate precipitation had low activity and this is likely to be related to the high concentration of residual surface carbonate that covers catalytic sites and inhibits reaction. For carbonate precipitation, increasing the Zr content to 1% resulted in a significant increase of activity, which is related to the decrease of surface carbonate. Increasing the Zr content up to 50% resulted in catalysts more active than ceria, but activity decreased as Zr content increased. This was in spite of increasing the number of oxygen vacancies, and this effect has been related to the decrease in the number of surface hydroxyl groups, which favours naphthalene adsorption. Ceria prepared by urea precipitation was markedly more active than that produced by carbonate precipitation. The urea-derived catalyst with 1% Zr is marginally more active than pure ceria, whilst for higher Zr contents activity was marginally lower. Two factors can account for these observations; they are the increase of oxygen vacancies contributing positively to activity and the opposing negative effect of decreasing the number of surface hydroxyl groups when the zirconium content increases.

© 2012 Elsevier B.V. All rights reserved.

1. Introduction

Naphthalene is a Polycyclic Aromatic Hydrocarbon (PAH), which is a specific group of pollutants classified within a wider group of pollutants known as Volatile Organic Compounds (VOCs). VOCs are now recognised as serious atmospheric pollutants [1]. Due to the more recent public and political attitudes towards atmospheric pollution, several legislative measures have been implemented to control VOC emissions. An example was the Gothenburg Protocol of 1999, which stated that VOC emissions needed to be reduced by at least 40% by 2010. VOCs are responsible for causing some illnesses [2], and they have also been implicated in the formation of ground level ozone [1] and photochemical smog [2].

Naphthalene has been detected as a waste product in many commercial and domestic applications, such as emissions from diesel exhaust [3]. Of the methods available for the removal of naphthalene, catalytic oxidation is the most efficient in terms of monetary cost and energy efficiency. For example, thermal incineration is an

option, but much higher treatment temperatures are required. It is also undesirable as the high temperatures can lead to the formation of nitrogen oxides (NO_x) and other toxic by-products, such as dioxins and dibenzofurans, if the process is not carefully controlled.

The catalytic total oxidation of PAHs has not been studied extensively when compared with other VOCs, but there are a number of reports describing the use of a range of catalysts [4]. Naphthalene has been commonly used as a suitable model PAH, and precious metal based catalysts (particularly Pd and Pt) are consistently active on a variety of supports. Zhang et al. reported that Pd and Pt catalysts supported on γ-Al_2O_3 were very active compared to other transition metals, such as W and Co [5]. The modification of 0.5 wt% Pt/γ-Al_2O_3 by 0.5 wt% vanadium was reported by Ndifor et al. [6] to improve activity; however, higher V loadings had a detrimental effect on activity due to the formation of crystalline V_2O_5.

In recent years, nanocrystalline ceria has been identified as being one of the most active catalysts for the total oxidation of naphthalene [7]. Previous studies have focussed on the influence of ceria preparation variables, with the aim of determining which catalyst features are required for naphthalene total oxidation. Factors such as crystallite size, surface area and oxygen defect concentration were all identified as having an important controlling influence

* Corresponding author.
  E-mail address: taylorsh@cardiff.ac.uk (S.H. Taylor).

[7,8]. Hence, the addition of platinum nanoparticles onto the surface of nanocrystalline ceria would be expected to improve the activity further. However, a recent study shows that adding platinum suppresses the activity when compared to ceria alone [9], and the same type of behaviour has also been observed for the addition of gold nanoparticles [10]. Therefore, a driving force to identify more active catalysts for PAH abatement exists, but it appears that the addition of precious metal nanoparticles to the active high surface area ceria is not an effective approach. Recently, we have found that copper doped ceria catalysts, where copper was fully incorporated into the ceria lattice, have better performance when compared to precious metal based catalysts [11]. For these catalysts, it was demonstrated that the surface oxygen defects were important for controlling naphthalene oxidation, since the addition of very low amounts of copper to non-ordered mesoporous ceria promotes the activity and selectivity to produce a very active catalyst for naphthalene total oxidation. Increasing the amount of oxygen defects has also been reported for the introduction of a range of other ions into the CeO_2 lattice [12], and the incorporation of Zr^{4+} ions is one of the most studied catalytic systems due to their extended use in vehicle exhaust after-treatment catalysts [13,14]. Accordingly, it has been reported recently that the addition of zirconium into the lattice of ceria improves the activity for naphthalene total oxidation [15], the catalytic activity for naphthalene oxidation over CeO_2-ZrO_2 mixed oxide catalysts being directly related to the catalyst redox properties. The sequence of reducibility of the catalysts followed the order: $Ce_{0.75}Zr_{0.25}O_2 > Ce_{0.50}Zr_{0.50}O_2 > Ce_{0.25}Zr_{0.75}O_2$, which was the same order as the catalytic activity. Therefore, it is of interest to know if incorporation of lower amounts of Zr^{4+} into the ceria lattice could lead to improved catalyst performance for PAH oxidation. Thus, the aim of the present study is to investigate the role of zirconium addition on a range of zirconia doped ceria catalysts prepared by coprecipitation and used for the catalytic combustion of naphthalene. Furthermore, we have investigated the influence of preparation route, and a comparison has been made of catalysts prepared by coprecipitation using urea and those precipitated with sodium carbonate.

2. Experimental

2.1. Catalyst preparation

The cerium/zirconium mixed oxides were synthesised using two different precipitation methods – one used urea as the precipitating agent and the other sodium carbonate. $(NH_4)_2Ce(NO_3)_6$ (Aldrich) was used as the cerium source and $ZrO(NO_3)_2 \cdot H_2O$ (Aldrich) was used as the zirconium source. The two series of catalysts were prepared with Ce/Zr molar ratios of 100/0, 99/1, 90/10, 80/20 and 50/50. The sample identifiers for the catalyst series are prefixed with U- or C-, which denotes precipitation using urea and carbonate respectively, and of the format $CeZrO_X$-a/b, where a and b relate to the molar percentage of cerium and zirconium respectively.

For the urea precipitated catalysts, urea (Aldrich, ACS reagent, 99–100.5%, 40 g), distilled water (200 mL) and the appropriate amounts of ammonium cerium(IV) nitrate (Aldrich, 99.99+ %) and zirconyl nitrate hydrate (Aldrich, 99%) were aged under reflux conditions with stirring in a round-bottomed flask for 24 h at 100 °C in the pH range 8–9. The resulting slurry was filtered, washed with deionised water and dried at 110 °C overnight. This was followed by calcination in static air at 500 °C for 6 h with a ramp rate of 10 °C min^{-1}. For the carbonate precipitated catalysts, 0.25 M solutions of zirconyl nitrate hydrate (Aldrich, 99%) and ammonium cerium(IV) nitrate (Aldrich, 99.99+ %), in proportions dependent on the desired Ce/Zr ratio, were combined and heated to 80 °C with stirring. Aqueous sodium carbonate solution (0.25 M) was then added dropwise until a pH of 8–9 was reached. This was then aged at 80 °C with stirring for 1 h. The precipitate was filtered, washed with distilled water and then dried at 110 °C overnight. The dried precursors were calcined for 3 h at 400 °C in static air with a ramp rate of 10 °C min^{-1}.

2.2. Catalyst characterisation

Surface areas were determined using the BET method and were performed using a Micromeritics Gemini 2360 instrument. The catalysts were degassed under an N_2 flow at 120 °C for 45 min prior to performing a five point analysis at −196 °C.

Powder X-ray diffraction (XRD) patterns were obtained using a PANalytical X'pert Pro diffractometer equipped with a Cu Kα X-ray source. Conditions of 40 kV and a current of 40 mA were used. Data were collected over the angular range of 10–80° 2θ. Crystallite sizes were calculated using the Scherrer method, by comparing the FWHM of diffraction peaks against a highly crystalline silicon standard.

Laser Raman spectra were obtained using a Renishaw Ramascope fitted with a Spectraphysics argon ion laser (λ = 514 nm) at a power of 20 mW. An Olympus BH2-UMA microscope was used for laser focussing. Scanning electron microscopy images were obtained using a Carl Zeiss EVO 40 scanning electron microscope fitted with backscattered and secondary electron detectors. For image collection using these detectors, variable working distances and probe currents were used. An EHT of 25 keV was used for all sample imaging, and samples were mounted on carbon adhesive discs. For energy dispersive X-ray (EDX) elemental analysis, the same microscope was use with a working distance of 9 mm and data was collected using an Oxford Instruments analyser.

Temperature programmed reduction (TPR) studies were carried out on a Micromeritics Autochem II 2920 with Cryocooler using 10% H_2 in Ar as the analyte gas, with a flow of 50 cm^3 min^{-1} over a temperature range of 50–800 °C. A sample mass of ca. 100 mg was used.

Diffuse reflectance infrared Fourier transform spectroscopy (DRIFTS) studies were carried out with a VERTEX 70 FTIR instrument operated with OPUS software. A Spectratech DRIFT high-temperature cell was filled with the powdered sample. The required gas flow (synthetic air or naphthalene in N_2) of 25 cm^3 min^{-1} was maintained by mass-flow controllers. Moisture free catalyst spectra were obtained after heating the sample at 150 °C for 30 min. Prior to the in situ adsorption/reaction measurements by DRIFTS at 250 °C, the samples were activated at 400 °C for 30 min in synthetic air flow. Each spectrum presents an average of 32 scans collected with a spectral resolution of 2 cm^{-1}. The spectra shown were obtained after subtraction of the features from the catalyst, recorded at 250 °C in He. Below 750 cm^{-1} the spectra showed specular reflections and, therefore, this region is not included in the discussion.

X-ray photoelectron spectroscopy (XPS) was performed using a Kratos Axis Ultra DLD photoelectron spectrometer fitted with a monochromatic Al source (photon energy = 1486.6 eV). Pass energies of 40 eV (high resolution scans) and 160 eV (survey spectra) were used over an analysis area of 700×300 μm. All spectra were calibrated to the C(1s) binding energy for adventitious carbon (binding energy = 284.7 eV). XPS data were analysed using CasaXPS software. Shirley background subtraction was applied to all the raw data. All peaks of the corrected plot were fitted with a Gaussian–Lorentzian shape function to peak fit overlapping features. Iterations were performed using the Marquardt method. Standard deviations were always lower than 1.5%.

2.3. Catalyst testing

The activity of the catalysts for naphthalene oxidation was determined using a fixed bed microreactor. Catalysts were tested in powdered form, using a ¼″ o.d. stainless steel reactor. The naphthalene was introduced using a heated generator regulated by a PID temperature controller. The reaction feed consisted of 100 vppm naphthalene in a gas stream of 20 vol.% O_2 in He. The total flow rate was 50 cm^3 min^{-1}, and catalysts were packed to a constant volume, to give a gas hourly space velocity of 135,000 h^{-1} for all studies. Analysis was performed on-line using a Varian 3400 gas chromatograph equipped with thermal conductivity and flame ionisation detectors. The catalytic activity was measured over the temperature range 100–350 °C in incremental steps, and temperatures were measured by a thermocouple placed directly into the catalyst bed. After a stabilisation time, three analyses were made at each temperature to ensure that steady state data were collected. After attaining steady state the reaction temperature was increased to the next value and the same procedure followed to determine each data point. Catalytic activity was expressed in two different ways. Naphthalene conversion was calculated from the difference between the moles of naphthalene in the reaction feed and those exiting the catalyst bed. Selectivity towards CO_2 was calculated as moles of naphthalene reacting to CO_2/total moles of naphthalene converted (taking into account the relative carbon numbers), then converted to a percentage. As total oxidation was the aim, activity was also calculated from moles of naphthalene converted to CO_2/moles of naphthalene in the inlet stream expressed as a percentage.

3. Results and discussion

In order to determine the extent of homogeneous gas phase reactions, a blank experiment was carried out using an empty reactor. CO_2 was detected at 350 °C and quantifiable at 375 °C, but the amount was very low. Additionally, ZrO_2, produced from both urea and carbonate precipitation, only demonstrated activity equivalent to the blank reaction and hence can be regarded as inactive for the total oxidation of naphthalene over the temperature range probed in this study.

Fig. 1A shows the catalytic activity for conversion of naphthalene to CO_2 for the range of catalysts prepared by precipitation with urea. Although U-CeZrO$_X$-99/1 was slightly more active than the U-CeO$_2$ parent catalyst, in general, there was similar catalyst activity when Zr was incorporated into the catalyst, except for the U-CeZrO$_X$-50/50 catalyst which showed lower performance than all the urea precipitated catalysts. It must be noted that for all these catalysts the selectivity was 100% at temperatures of 250 °C and above. Below 250 °C the catalysts did not show 100% CO_2 selectivity, and although CO_2 was always by far the major product, low levels of other products, such as phenanthrene, naphthalene dione, dimethyl phthalate, benzene, alkyl benzenes, benzaldehyde, toluene and xylenes were also identified.

The activity for naphthalene total oxidation is shown in Fig. 1B for the C-CeZrO$_X$ catalysts (precipitated using carbonate). All C-CeZrO$_X$ catalysts displayed higher catalytic activities compared to pure C-CeO$_2$. Hence, in this series of catalysts the addition of Zr has a positive effect on promoting activity. The largest increase of activity was produced by the addition of 1% Zr whilst adding larger quantities systematically decreased activity compared with the catalyst containing 1% Zr. Additionally, the selectivity towards CO_2 for the C-CeZrO$_X$ series clearly improved when incorporating Zr. All the Zr-containing samples reached 100% CO_2 selectivity above 225 °C. However, the C-CeO$_2$ only showed 100% CO_2 selectivity at 275 °C coupled with a low naphthalene conversion of 17%. Therefore, the addition of Zr to CeO$_2$ improves the naphthalene conversion but
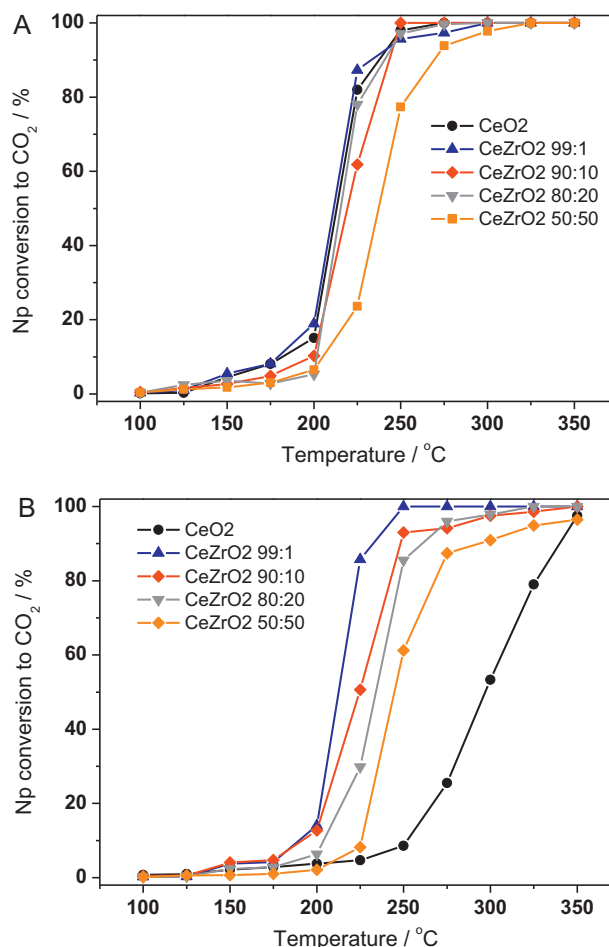

Fig. 1. Catalytic activities for the total oxidation of naphthalene. Temperature range: 100–350 °C. GHSV = 135,000 h^{-1} for all experiments; 100 vppm naphthalene in air. Numbers in the legend refer to Ce:Zr atomic weight ratios. A. U-CeZrO$_X$; B. C-CeZrO$_X$.

also the CO_2 selectivity when the catalyst is prepared by precipitation with carbonate. When CO_2 selectivity was less than 100%, the same type of partially oxidised products mentioned earlier were also formed over the carbonate precipitated catalysts.

Comparing the activity of urea- and carbonate-precipitated CeZrO$_X$ catalyst series, it was found that whilst the CeO$_2$ parent catalysts show very different behaviour, as has been previously reported [10], once zirconia is added both CeZrO$_X$ series did not exhibit such different catalytic performance (see Fig. 1 and specific activity in Table 1), and the best catalysts were the ones prepared with 1% Zr content for both series. What is clearly different for the 2 sets of catalysts is the magnitude of improvement of catalyst performance by the addition of Zr. The increase of activity on Zr addition was relatively minor for the catalysts precipitated by urea, whilst the increase of activity was very significant for carbonate precipitated catalysts.

Table 1 shows a summary of some of the characterisation data for the series of catalysts precipitated using carbonate and urea. In the urea series the surface areas are similar for all catalysts (ranging from 117 to 142 m^2 g^{-1}) without a clear correlation between Zr loading and catalyst surface area. For the catalysts prepared by precipitation via carbonate, the surface area of catalysts containing Zr, no matter what the Zr content, was increased by a factor of at least 2 when compared to pure C-CeO$_2$ (110–140 m^2 g^{-1} in Zr-containing catalysts compared with 56 m^2 g^{-1} for pure ceria). As will be shown later, the amount of surface carbon for C-CeO$_2$ was much higher than for other catalysts and this could relate to the very

Table 1
Catalyst characterisation parameters determined during this study.

Catalyst	Surface area (m²/g)[a]	Crystallite size (nm)[b]	Lattice strain (%)[b]	Lattice parameter (Å)[b]	Raman FWHM (cm⁻¹)[c]	H_2 consumption (mmol/g cat)[d]	Specific activity 10^{-5} at 225 °C (gNp/h/m²)
U-CeO₂	120	7.4	2.1	5.412	20	0.67	21.7
U-CeZrOₓ-99/1	117	6.8	2.2	5.405	24	0.72	23.6
U-CeZrOₓ-90/10	135	5.5	2.7	5.394	35	1.0	14.6
U-CeZrOₓ-80/20	142	5.0	2.9	5.375	43	1.4	17.4
U-CeZrOₓ-50/50	111	2.3	6.3	5.317	71	1.6	6.6
C-CeO₂	56	6.5	2.3	5.411	36	1.3	2.8
C-CeZrOₓ-99/1	144	6.5	2.4	5.411	31	0.55	19.2
C-CeZrOₓ-90/10	125	6.5	2.4	5.394	42	0.58	13.0
C-CeZrOₓ-80/20	112	6.2	2.2	5.377	55	0.96	8.5
C-CeZrOₓ-50/50	131	4.3	3.3	5.317	70	1.2	2.0

[a] By BET analysis.
[b] By XRD analysis. Cubic system, $Fm3m$ (225).
[c] By Raman spectroscopy.
[d] By TPR.

low surface area. Surprisingly, the addition of only 1% Zr increased the surface area of the carbonate precipitated catalyst to the value reached for ceria prepared *via* urea precipitation. As will be shown later, the Zr addition facilitates the removal of surface carbonates during the calcination step, but it must also be highlighted that the carbonate catalyst was also calcined at a slightly lower temperature than the urea catalyst. Finally, we note that both preparation methods led to similar final surface areas for the CeZrOₓ catalysts.

Average crystallite sizes were calculated from the powder XRD data by using the Scherrer equation, and the values are shown in Table 1. The inclusion of Zr generally led to a decrease in crystallite size. In the urea series, all the samples showed smaller crystallites than pure CeO₂, and these values decreased directly as the Zr content increased. A similar trend was also seen for the carbonate series of catalysts, which displayed similar crystallite sizes to the urea precipitated series. There was no direct relationship between crystallite size and surface area and this suggests that there may be some contribution to X-ray line broadening from disorder or there may be differences of catalyst porosity.

Powder XRD patterns for the urea and carbonate series of catalysts are displayed in Fig. 2. For both series, without Zr addition the phase identified was cubic fluorite CeO₂. The cubic fluorite phase observed in both series has reflections originating mainly from the (111), (200), (220) and (311) lattice planes [16]. Upon incorporation of Zr the patterns for both series of catalysts appear to be similar, with the exception of line broadening discussed earlier (Table 1). A successive loss of crystallinity, indicated by increased background diffraction, was also observed when the Zr content was increased. There were no new diffraction peaks evident as the Zr content was increased, but a shift in peak position was observed. This suggests that Zr was incorporated into the lattice of CeO₂ to form a solid solution. For low levels of Zr it is difficult to unequivocally identify formation of a solid solution, as a consequence of the expected small decrease of the lattice parameter and the broad diffraction peaks. The introduction of higher levels of Zr into the lattice reduced the observed d-spacing for both urea and carbonate precipitated CeZrOₓ catalysts, and hence reduced the lattice parameter (Table 1). This is not surprising when one considers that ZrO₂ has a smaller lattice parameter than CeO₂, the ionic radius of Zr⁴⁺ (0.084 nm) being smaller than that of Ce⁴⁺ (0.097 nm). Increasing the Zr content decreased the crystallite size, and it is possible to determine a measure of the relative contributions towards X-ray line broadening from both crystallite size and from lattice strain [17]. The contribution to line broadening due to lattice strain seemed to increase with increasing Zr content, consistent with the presence of smaller crystallites [15] (Fig. 2).

Laser Raman spectroscopy is a useful characterisation technique for solid catalysts. Some of the variables that may influence

the Raman spectra are internal strain, which shifts and broadens the bands, nonstoichiometry and other crystal defects which also broaden Raman bands [18–20], and specifically for nanoscale solids, the phonon confinement effect that can shift, widen and reduce the symmetry of the vibrational bands [21]. In this work, the main influence on Raman data were expected to originate from the substitution of Zr into ceria, already observed by XRD analysis. Hence changes in crystallite size, structure and defect density, may all affect the Raman spectra. It has been established that six
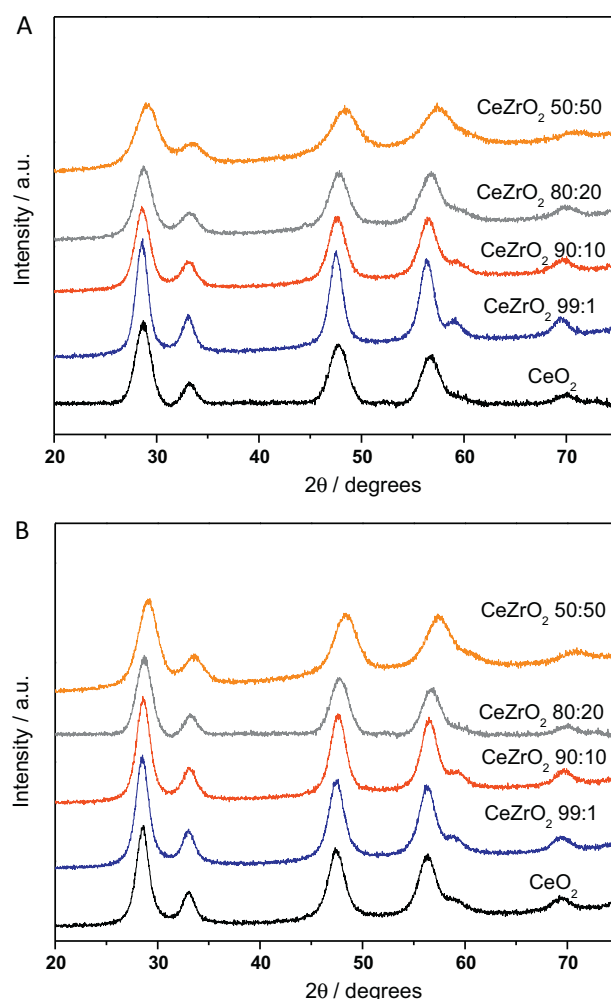
Fig. 2. Powder XRD patterns obtained for all ceria catalysts. A. U CeZrOₓ; B. C CeZrOₓ.

A

B
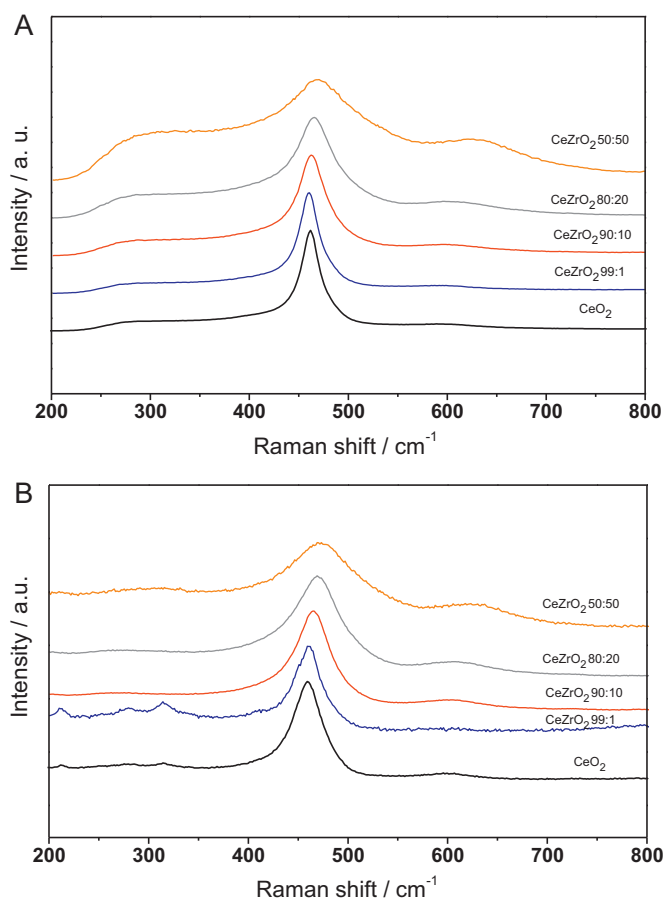
Fig. 3. Laser Raman spectra of catalysts. A. U CeZrOX; B. C CeZrOX. Laser $\lambda = 514$ nm. Intensity of CeO_2 (*i.e.* 100–0) spectrum halved for clarity of other less intense spectra.

Raman-active modes of A1g + 3Eg + 2B1 g symmetry are observed for tetragonal ZrO_2 (space group P42/nmc), whilst for the cubic fluorite structure (space group *Fm3m*) only one *F2g* mode centered at around 465 cm^{-1} is Raman-active for CeO_2 [22]. For these samples, it is apparent from their Raman spectra that they are in the cubic form, and do not show any indication of modification to the tetragonal form. No Raman lines due to ZrO_2 could be observed, which is consistent with XRD measurements. However, the appearance of weak bands at *ca.* 620 cm^{-1} has been related to the presence of O vacancies [23].

For both series of catalysts the major Raman band shifted towards higher frequencies when increasing the Zr content. The shift of the F2 g Raman frequency to higher values at higher zirconia ratios suggests the incorporation of Zr^{4+} into the CeO_2 lattice, resulting in a decrease of lattice parameter [22]; consistent with XRD results. In addition, the presence of a peak at *ca.* 300 cm^{-1} at higher Zr content implies distortion of the oxygen lattice, see Fig. 3. The FWHM values, calculated from the Raman band at a frequency of *ca.* 460 cm^{-1} (Table 1), showed a progressive increase in magnitude when the Zr content was increased for both the urea and carbonate series of catalysts. The only exception was for the C-CeZrO$_X$-99/1 catalyst for which the value slightly decreased compared to pure C-CeO$_2$. The Raman FWHM value is related inversely to crystallite size, whilst it is also related directly to internal strain [24] and to the concentration of crystal defects (mainly oxygen vacancies [25,26]). Therefore, the increase of the Raman FWHM in the urea and carbonate catalyst series would be in agreement with the generally decreasing crystallite size determined by XRD. However, the relationship between FWHM and crystallite size is not linear, as it is reported to be for pure CeO_2, if crystallite size is

the only factor controlling the Raman peak FWHM [27]. Thus, the broadening of peaks can be attributed to an increased concentration of crystal defects [20,24], and/or an increase of internal strain arising from the inclusion of Zr. This effect has also been observed in other studies, and has been explained by the readiness of CeO_2 to form oxygen vacancies and the ability of Zr to enhance this process [25,26]. Accordingly, the more apparent presence of a broad band near 600 cm^{-1}, due to a LO mode of ceria at higher Zr contents for both catalyst series, shows that greater substitution of zirconium into the ceria lattice gives rise to an increasing amount of oxygen vacancies. Similar behaviour has been obtained for both series of CeZrO$_X$ catalysts. However, although Zr incorporation into the CeO_2 lattice promotes the formation of oxygen vacancies, for higher Zr contents activity was reduced. Therefore, the number of oxygen vacancies does not seem to be the key parameter controlling the activity of CeZrO$_X$ catalysts as has been reported for CeO_2 [8] and copper doped CeO_2 [11] catalysts, and hence other catalyst properties must also be considered.

Temperature programmed reduction in a flow of hydrogen up to 700 °C was used to characterise the calcined catalysts and probe redox properties. In this temperature range bulk CeO_2 is not expected to be reduced [28], but surface capping oxygen species are. The TPR profiles for the urea precipitated series of catalysts show two general trends (Fig. 4A). Firstly, the incorporation of Zr caused an increase in the amount of H_2 consumption, as peak areas for all CeZrO$_2$ catalysts were greater than those observed for CeO_2 (Table 1). Secondly, increasing Zr content caused a marginal increase in the temperature of the maximum for the reduction peak. The main reduction peak for U-CeO_2 was at 510 °C and this slightly increased to *ca.* 540 °C as the Zr content was increased to 50%. It must also be noted that the quantity of H_2 consumed increased with increasing Zr concentration, and hence the extent of reduction increased with increasing Zr content. Thus, there appears to be an inverse relationship between the amount of labile oxygen and catalytic activity for catalysts with similar surface areas, which is a totally unexpected result. Indeed, it has been found in this work that the most active catalyst, U-CeZrO$_X$-99/1, was one of the least reducible catalysts in terms of H_2 consumption. Conversely, Bampenrat et al. [15] reported that for naphthalene total oxidation over CeZrO$_X$, higher catalytic activity was achieved as reducibility of the catalysts increased, for Zr contents ranging from 25% to 75%. Both the different range of Zr substitution studied and the use of a Ce^{3+} salt precursor by Bampenrat et al. to prepare the catalyst could influence the behaviour and explain differences from our observations.

Temperature programmed reduction profiles are shown for the calcined carbonate precipitated series of catalysts in Fig. 4B. The same conclusions to those found for the urea precipitated series can be reached, since similar profiles were obtained. Thus, total H_2 consumption was increased and the main reduction peak was shifted to higher temperature at higher Zr content. An exception was found in the case of the pure C-CeO_2 catalyst where a high amount of surface carbonates (see BET values and DRIFTS data) could lead to a higher H_2 consumption. It is also observed that for the C-CeZrO$_X$-50/50 catalyst the broad reduction peak with a shoulder at 350 °C was replaced by two distinct reduction peaks. Since both peaks could be related to the reduction of two different capping oxygen species, the peak at lower temperature could be clearly related to the amount of Zr content in the crystalline structure and to the increasing amount of oxygen vacancies detected by Raman spectroscopy as Ce substitution increased. Again, an inverse relationship is observed between the ease of catalyst redox properties and catalytic activity.

The surface chemistry and the composition of the catalysts were probed using XPS. Comparison of the Ce:Zr ratio between the U- and C-CeZrO$_X$ series of catalysts showed that the surface ratios were

Table 2
Ce:Zr bulk and surface ratios determined by EDX and XPS, respectively, for urea and carbonate series of catalysts.

| Catalyst	Bulk Ce:Zr ratio (at.%)	Surface Ce:Zr ratio (at.%)	Surface Ce^{3+} (at.%)	Surface C (at.%)	Relative O$_\alpha$ (at.%)	Relative O$_\beta$ (at.%)
U–CeO$_2$			34	22	54	46
U–CeZrO$_X$-99/1	99.3:0.7	99:1.0	37	19	38	62
U–CeZrO$_X$-90/10	93:7	94:6	36	21	28	72
U–CeZrO$_X$-80/20	85:15	88:12	38	22	38	62
U–CeZrO$_X$-50/50	58:42	64:36	41	21	44	56
C–CeO$_2$			26	27	37	63
C–CeZrO$_X$-99/1	99:1.0	99:1.1	28	22	54	46
C–CeZrO$_X$-90/10	92:8	94:6	27	21	40	60
C–CeZrO$_X$-80/20	83:17	87:13	23	22	42	58
C–CeZrO$_X$-50/50	61:39	62:38	24	19	40	60

very similar to those expected from the bulk composition (Table 2), and none of the methods favoured enrichment of Ce at the surface over the bulk (determined by EDX).

XPS was also used to investigate surface oxidation states and the relative amount of some components. Firstly, it was confirmed that the C-CeO$_2$ catalyst presented a higher amount of surface carbon (Table 2), which could explain the markedly lower surface area and activity of these samples. These data are in agreement with the presence of a higher amount of surface carbonate, as will be shown

later by DRIFTS. Similar amounts of surface carbon were found for the other catalysts. On the other hand, an increased concentration of Ce^{3+} compared with Ce^{4+} has been previously proposed to be detrimental to the activity of a ceria catalyst for the total oxidation of naphthalene [7]. The relative amount of Ce^{3+} and Ce^{4+} was calculated from the curve-fitted Ce(3d) spectra (Fig. 5), as described in the literature [29], and the results are shown in Table 2. All the samples analysed contained predominantly surface Ce^{4+}, with different amounts of Ce^{3+} depending on the preparation method and the Zr content. It can be observed that generally the urea precipitated series contained a higher amount of Ce^{3+} compared to carbonate
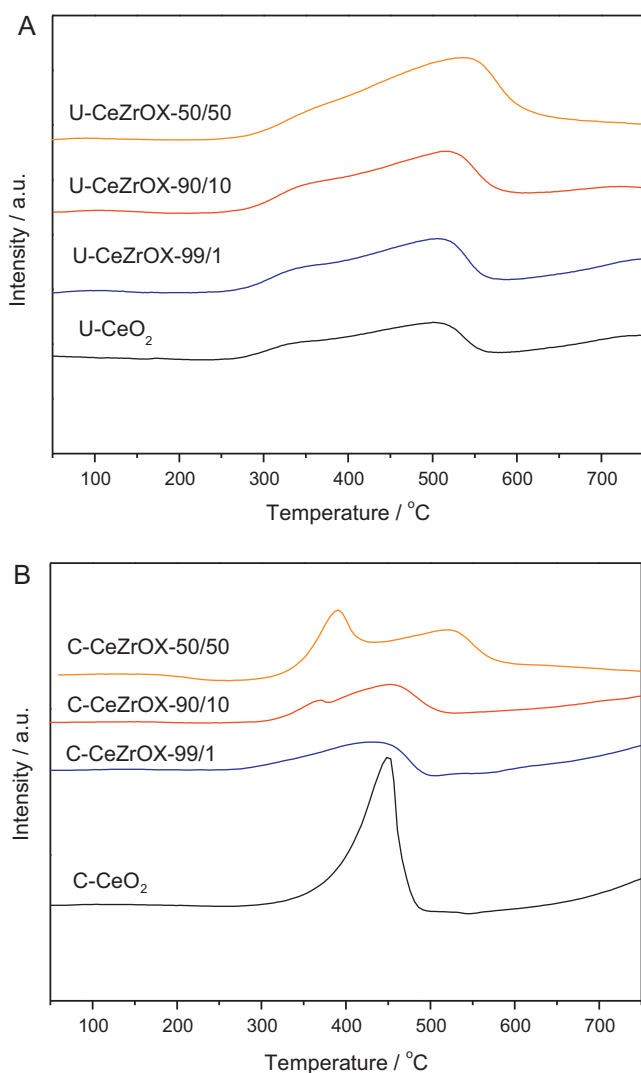
Fig. 4. Temperature Programmed Reduction data for ceria catalysts. A. U-CeZrO$_X$; B. C-CeZrO$_X$.
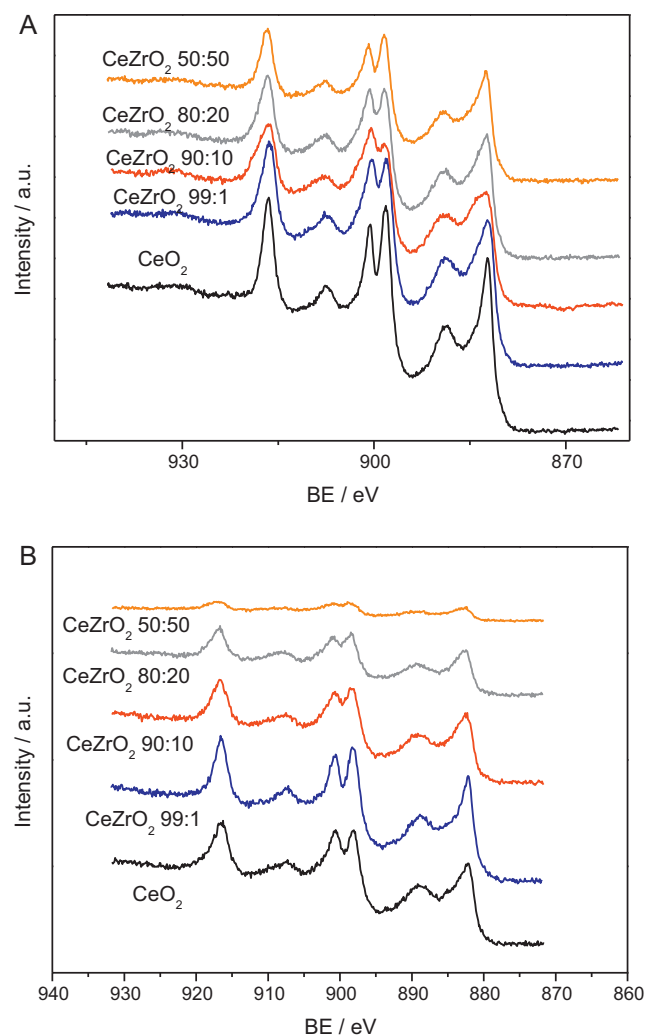
Fig. 5. XPS spectra of Ce 3d for ceria catalysts. A. U-CeZrO$_X$; B. C-CeZrO$_X$.
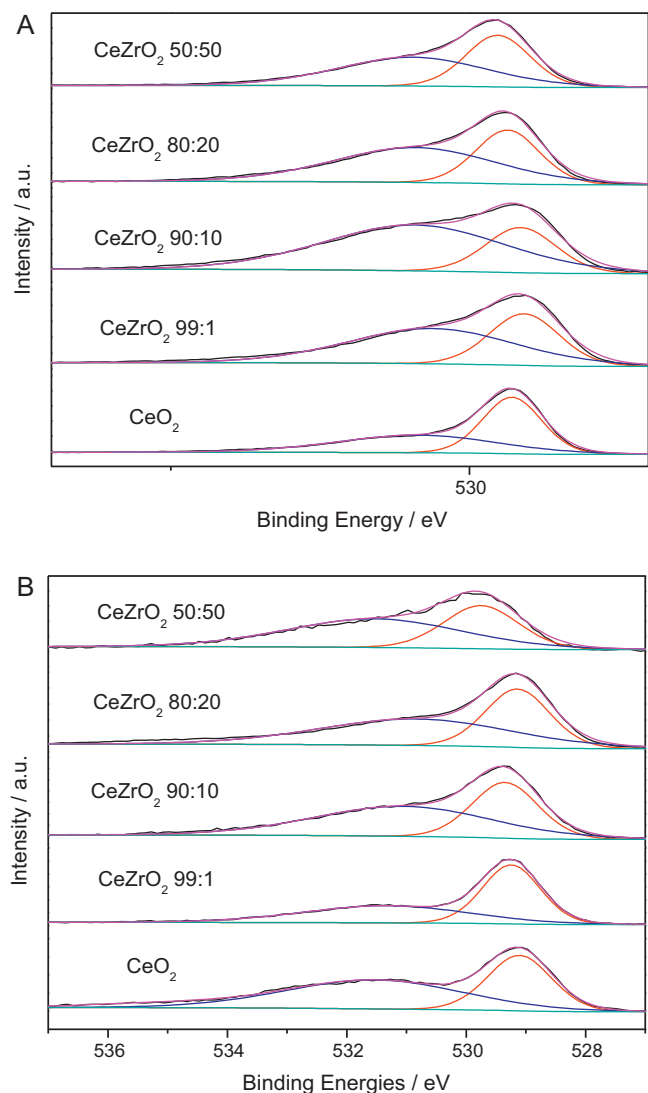
Fig. 6. XPS spectra of O1s for ceria catalysts. A. U-CeZrO$_X$; B. C-CeZrO$_X$.

Fig. 7. DRIFT spectra after 30 min at 400 °C in synthetic air for A) U-series catalysts and B) C-series catalysts.

precipitated catalysts. This could indicate a higher concentration of surface oxygen vacancies for the urea catalysts, although both series have roughly similar activity for the same Zr content. Both series of catalysts presented similar surface Ce^{3+} concentrations regardless of the Zr content. Therefore, again it is not possible to establish any clear relationship between the performance of these catalysts and the amount of Ce^{3+} on the catalyst surface. The Zr(3d) spectra were also analysed for both the urea and carbonate series (not shown). The peak binding energies did not significantly shift when the Ce:Zr ratio was altered.

The O(1s) spectra clearly show two surface oxygen species (Fig. 6). According to Galtayries et al. [30], the binding energy of 529–530 eV, denoted as O$_\alpha$, is characteristic of the lattice oxygen (O^{2-}), and the binding energy in the region of 531–533 eV, denoted as O$_\beta$, may be assigned to defect oxide or to surface oxygen ions with low coordination. There may be a contribution to the 531–533 eV peak from either surface hydroxyl or carbonate species [31]. The relative amounts of the different oxygen species are summarised in Table 2. The presence of surface oxygen vacancies, surface carbonates and hydroxyl species are strongly dependent on both the preparation method and the Zr content, and hence the intensity of the O$_\beta$ peak cannot be solely linked to the presence of any of these oxygen species. Oxygen vacancies, hydroxyl surface groups and surface carbonate species influence the catalyst
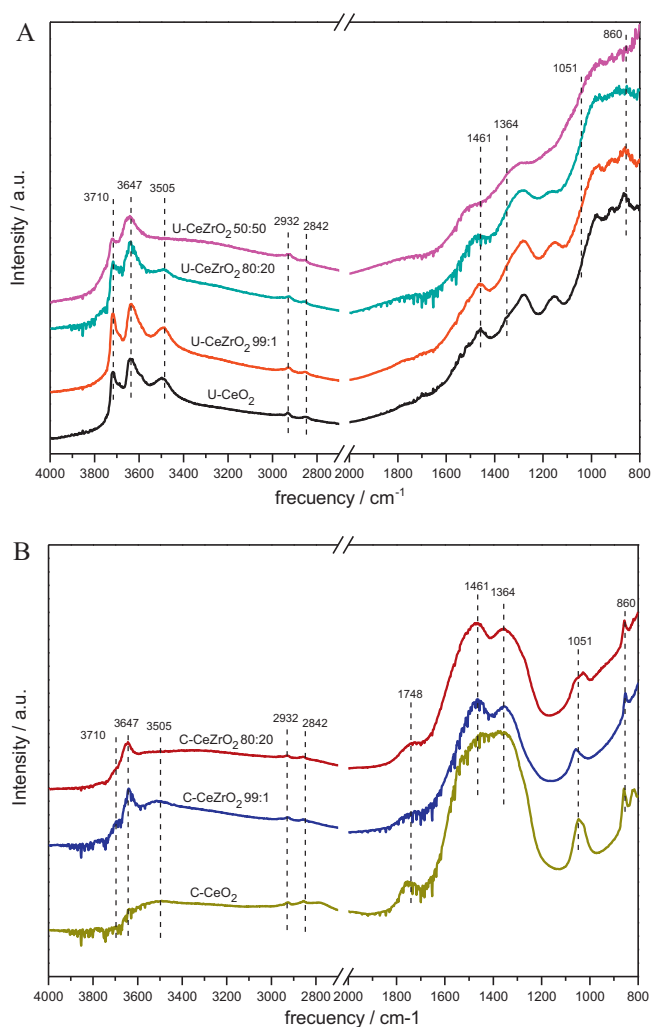
performance in different ways, and this will be discussed below. For example, whilst oxygen vacancies seem to increase the activity of the catalyst [9] and the effect of hydroxyl groups are also favourable, the presence of surface carbonate clearly leads to less active catalysts [11].

In order to probe the presence of surface carbonates and hydroxyl groups, as well as reaction intermediates, DRIFTS experiments were conducted on representative catalysts. DRIFTS spectra of all the catalysts collected after oxidative activation under synthetic air at 400 °C for 30 min are shown in Fig. 7. These spectra are divided into three regions characteristic of different vibrations: 4000–3200 cm^{-1} (OH vibrations), 3200–2700 cm^{-1} (CH vibrations) and 2000–800 cm^{-1} (CO/CC vibrations). Due to the nature of the DRIFTS experiments it was only possible to obtain qualitative data, and hence discussion of the results is also only qualitative.

For the urea precipitated catalysts the spectra of all catalysts show three bands in the OH vibrational region (Fig. 7A). The band at 3710 cm^{-1} was assigned to mono-coordinated OH (type I) groups; the band at 3647 cm^{-1} was assigned to bridging OH (type II) groups; and a broad band centered at 3505 cm^{-1} was assigned to hydroxyl groups of a ceria oxyhydroxide phase [32,33]. The latter species are present in all the U-CeZrO$_2$ series of samples, except for the catalyst with 50% molar ratio of zirconium and it seems that the addition of Zr in the U-series catalysts reduces the concentration of all surface hydroxyl groups.

On the contrary, carbonate precipitated catalysts present different features related to the surface hydroxyl groups. The C-CeO$_2$ catalyst did not show the presence of the characteristic OH bands, and the addition of Zr promoted the appearance of weak bands at 3647 cm^{-1} (type II OH) and 3710 cm^{-1} (type I OH), which are slightly more apparent at lower Zr content (Fig. 7B).

The most marked influence of the precipitation method on the surface chemistry of the catalyst can be observed in the CC/CO vibration region. All catalysts prepared with carbonate (C-CeZrO$_2$ series, Fig. 7B) show two broad bands at 1461 and 1364 cm^{-1}, and 2 peaks at 1051, and 860 cm^{-1}. Previously these have been assigned to bulk-type polydentate carbonates [32,34,35]. The C-CeO$_2$ catalyst contains the highest amount of residual surface carbonate species, whilst the incorporation of just 1% of Zr into the CeO$_2$ lattice reduces the formation of carbonates during the preparation process. This beneficial behaviour persists when the amount of Zr is increased. Interestingly, the reduction of surface carbonate on the addition of zirconia is mirrored by reduction of surface sodium species identified by XPS. C-CeO$_2$ had 3.5 at.% sodium on the surface, reducing to 1.0–1.5 at.% when zirconium was added. Finally, a bridged carbonate band is also visible in the spectra of the C-CeZrO$_2$ series of catalysts at 1748 cm^{-1} [34].

Catalysts prepared by the urea precipitation method present residual peaks in this region, with some shifts in the position of the peaks. This is most likely associated with changes in the coordination of the corresponding carbonates on the surface, but their detailed analysis is beyond the scope of this manuscript. Detectable peaks are also present in the CH region in the spectra of all catalysts at 2932 and 2842 cm^{-1} (Fig. 7A and B). According to the literature, these peaks can be assigned to residual bidentate or bridged formate species [33].

DRIFTS experiments were also conducted at 250 °C in the presence of naphthalene in a flow of N$_2$, in order to study the adsorption of naphthalene over the catalyst surface, as this is potentially the first step in the oxidation reaction. Spectra of all catalyst samples after 90 min exposure are shown in Fig. 8A and B.

The U-CeZrO$_2$ catalyst series (Fig. 8A) present notable features in all three regions of the DRIFTS spectra. In the OH stretching region, peaks at 3710, 3647 and 3505 cm^{-1} have mostly disappeared, and two negative bands assigned to singly and doubly coordinated hydroxyls, centred at 3697 and 3620 cm^{-1} respectively, are present. These negative peaks indicate that the corresponding surface hydroxyls are consumed by either adsorption or reaction of naphthalene. Two broad bands around 1540 cm^{-1} and 1405 cm^{-1} are present in the CC/CO stretching region and can be assigned to surface naphthoate species [36], which are produced by naphthalene chemisorption on the hydroxyl groups. These naphthoate species could represent one of the modes of adsorption of naphthalene on CeZrO$_2$ and at the same time, the first step towards naphthalene oxidation. In addition, two sharp peaks are present at 1371 and 1358 cm^{-1}, which can be assigned to bidentate and bridged formates [33] due to the partial oxidation of naphthalene. Furthermore, partially oxidised phthalate species are observed due to the presence of weak vibrational peaks at 1150 and 1082 cm^{-1} [37,38]. Finally, four well resolved peaks in the CH region can be assigned to naphthalene adsorption (3070 cm^{-1}) and formate sub-products of naphthalene oxidation (2935, 2854, 2721 cm^{-1}) [33], which are consistent with the presence of all the species discussed above. The formation of partial oxidation products on the surface in the absence of gas phase oxygen indicates that lattice oxygen is active for naphthalene oxidation *via* a Mars-van Krevelen type mechanism. U-CeZrO$_X$-99/1 and U-CeZrOx-80/20 catalysts present the same peaks and intensities as the U-CeO$_2$ catalyst, whilst U-CeZrOx-50/50 shows a decrease of intensity in the CH stretching region. These observations correspond to decreased concentrations of adsorbed naphthalene and oxidation products (formates), as well
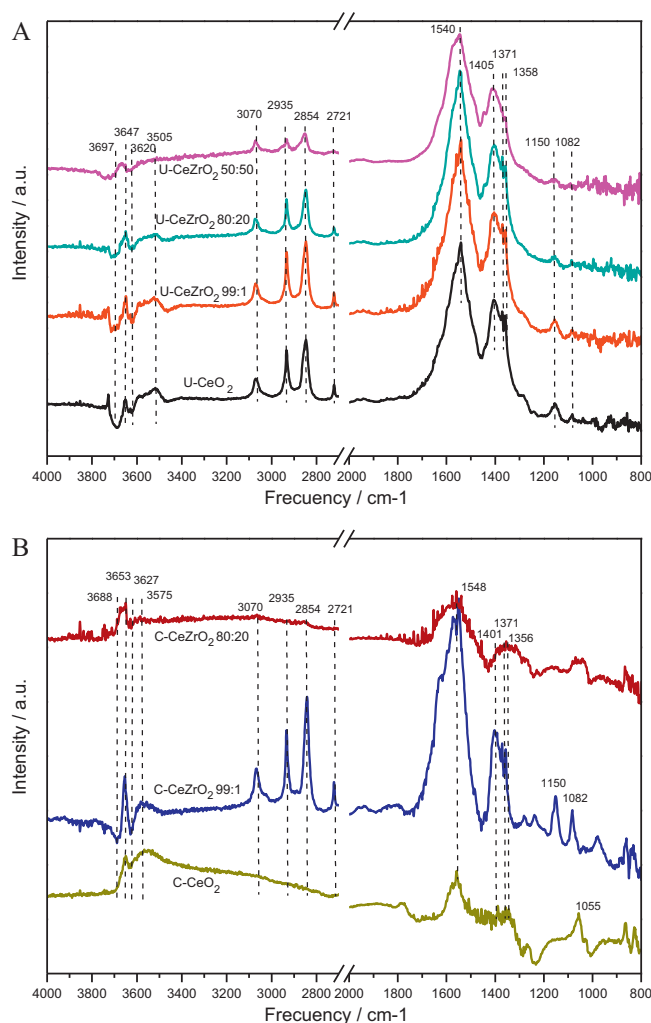

Fig. 8. DRIFT spectra after 90 min at 250 °C in naphthalene/N$_2$ for (A) U-series catalysts and (B) C-series catalysts.

as the depletion of the two narrow peaks at 1371 and 1358 cm^{-1} that are also characteristic of formates. The U-CeZrOx catalysts showed broadly the same activity, expressed as naphthalene conversion to CO$_2$ (Fig. 1A), except for the catalyst with a 50% molar ratio of Zr which showed a slight reduction of activity. It seems that increasing amounts of Zr content (50/50) could reduce the number of surface hydroxyl groups that take part in the naphthalene adsorption and also in the oxidation processes. This fact could explain a decreasing catalytic activity of CeZrOx at increasing Zr content, despite of the greater amount of oxygen vacancies detected by Raman and TPR analysis.

The C-CeZrOx series of catalysts present completely different features in the DRIFTS spectra (Fig. 8B) when compared with the U-series of catalysts discussed above. The C-CeO$_2$ sample only shows a residual peak in the CC/CO vibration region at 1548 cm^{-1} corresponding to a low concentration of adsorbed naphthalene on the catalyst surface. This sample also presents very low catalytic activity compared with the rest of the catalysts (Fig. 1B). Hence, the presence of a very high amount of residual carbonate, blocking and/or decreasing the amount of hydroxyl surface groups and porosity, could explain the very low activity of this catalyst.

As previously discussed, the addition of just 1% Zr significantly increases the activity of the carbonate precipitated catalyst. This can be explained by considering the DRIFTS spectrum of the catalyst at 250 °C in the presence of naphthalene in N$_2$, as it is completely different to the one obtained for C-CeO$_2$ and similar

to the U-series spectra, showing negative OH peaks related to the consumption of hydroxyl groups. The presence of the two characteristic bands for surface naphthoate species around 1540 and 1405 cm^{-1}, the phthalate vibrations at 1150 and 1082 cm^{-1} and the formate peaks in both CC/CO and CH stretching regions are also observed. As discussed for the U- CeZrOx series, the presence of surface hydroxyl groups for naphthalene adsorption seems to be a factor of paramount importance for the development of a very active catalyst for naphthalene total oxidation. Finally, the introduction of more Zr into the CeO$_2$ lattice again leads to a less active catalyst. The C-CeZrOx-80/20 catalyst shows a DRIFTS spectrum more similar to that observed for the C-CeO$_2$ catalyst than for C-CeZrOx-99/1, since few characteristic vibrational peaks due to naphthalene adsorption and reaction were detected. This behaviour in the C-CeZrOx-80/20 catalyst could be related to two opposite effects of Zr in the CeO$_2$ lattice: i) removal of carbonate species from the ceria surface leading to a catalyst with surface properties and catalytic activities similar to urea precipitated samples (only prevalent in samples with Ce:Zr ratios up to 90:10) and ii) the presence of hydroxyl groups which favours the adsorption and activation of naphthalene, and consequently leads to enhanced catalytic activity.

4. Conclusions

The addition of Zr to CeO$_2$ has been shown to be beneficial for the total oxidation of naphthalene, regardless of the preparation method employed. CeZrOx catalysts have been prepared by co-precipitation using two precipitating agents: sodium carbonate and urea. The factors affecting the catalytic activity are complex and these are: oxygen vacancies, surface area, the presence of carbonates and hydroxyl groups on the surface of the catalysts and possibly the presence of inactive bulk ZrO$_2$. Pure ceria prepared by carbonate precipitation had low activity and this is likely to be related to the high concentration of residual surface carbonate that covers catalytic sites and inhibits reaction. For carbonate precipitation, increasing the Zr content to 1% resulted in a significant increase of activity, which is likely to be related to the decrease of surface carbonate. Further increasing Zr content resulted in catalysts more active than carbonate precipitated ceria, but decreased activity relative to the catalyst containing 1% Zr. This was in spite of increasing the number of oxygen vacancies, and is related to the decrease in the number of surface hydroxyl groups, which favour the adsorption of naphthalene.

Pure ceria prepared with urea precipitation showed high catalytic activity, markedly higher than that obtained with carbonate precipitation. The catalyst with 1%Zr is marginally more active than pure ceria, whilst for Zr contents of 10 and 20% activity was marginally lower. Two factors can account for these observations: the increase in oxygen vacancies contributing positively to activity, and the opposing negative effect of a decrease in the number of surface hydroxyl groups when the zirconium content increases. The catalysts with a 50% ZrO$_2$ loading showed much lower catalytic activity than the rest of the urea prepared catalysts. This behaviour can be explained by the decrease in surface hydroxyl groups and possibly by increased formation of inactive ZrO$_2$.

References

[1] M.S. Jennings, M.A. Palazzolo N.E. Krohn, R.M. Parks, R.S. Berry, K.K. Fidler, Pollution Technology Review (Noyes Ed.), 1985, p. 121.
[2] O. Tolvanen, J. Nykanen, U. Nivukoski, M. Himanen, A. Veijanen, K. Hanninen, Waste Management 25 (2005) 427–433.
[3] H. Reinecke, R. Vetter, J. Holtz, H. Drexler, S. Diamond, R. Knoche, R.W. Luth, J. Lahaye, S. Boehm, P.H. Chambrion, P. Ehrburger, Combustion and Flame 104 (1996) 199–207.
[4] E.N. Ntainjua, S.H. Taylor, Topics in Catalysis 5 (2009) 528–541.
[5] X.W. Zhang, S.C. Shen, L.E. Yu, S. Kawi, K. Hidajat, K.Y. Simon Ng, Applied Catalysis A 250 (2003) 341–352.
[6] E.N. Ndifor, T. Garcia, S.H. Taylor, Catalysis Letters 110 (2006) 125–128.
[7] T. Garcia, B. Solsona, S.H. Taylor, Catalysis Letters 105 (2005) 183–189.
[8] A. Aranda, J.M. Lopez, R. Murillo, A.M. Mastral, A. Dejoz, A.I. Vazquez, B. Solsona, S.H. Taylor, T. Garcia, Journal of Hazardous Materials 171 (2009) 393–399.
[9] E.N. Ntainjua, T.E. Davies, T. Garcia, B. Solsona, S.H. Taylor, Catalysis Letters 141 (2011) 1732–1739.
[10] B. Solsona, T. García, R. Murillo, A.M. Mastral, E.N. Ntainjua, C.E. Hetrick, M.D. Amiridis, S.H. Taylor, Topics in Catalysis 52 (2009) 492.
[11] A. Aranda, E. Aylón, B. Solsona, R. Murillo, A.M. Mastral, D.R. Sellick, S. Agouram, T. García, S.H. Taylor, Chemical Communications 48 (2012) 4704–4706.
[12] L. Li, F. Chen, J.-Q. Lu, M.-F. Luo, Journal of Physical Chemistry A 115 (2011) 7972.
[13] Q.Y. Wang, B. Zhao, G.F. Li, R.X. Zhou, Environmental Science and Technology 44 (2010) 3870.
[14] J. Guo, S. Yuan, M. Gong, M. Shen, J. Zhong, Y. Chen, Journal of Rare Earths 25 (2007) 179.
[15] A. Bampenrat, V. Meeyoo, B. Kitiyanan, P. Rangsunvigit, T. Rirksomboon, Catalysis Communications 9 (2008) 2349–2352.
[16] M. Teng, L. Luo, X. Yan, Microporous and Mesoporous Materials 119 (2009) 158–164.
[17] C. Suryanarayana, M.G. Norton, X-Ray diffraction. A Practical Approach, Plenum Press, New York, 1998.
[18] J.W. Ager, D.K. Veirs, G.M. Rosenblatt, Physical Review B 43 (1991) 6491–6499.
[19] W.F. Zhang, Y.L. He, M.S. Zhang, Z. Yin, Q. Chen, Journal of Physics D 33 (2000) 912–916.
[20] L.A. Falkovsky, J. Camassel, Physica B 284–288 (2000) 1145–1146.
[21] S. Askrabic, R. Kostic, Z. Dohcevic-Mitrovic, Z.V. Popovi, Journal of Physics: Conference Series 92 (2007) 012042.
[22] G. Vlaic, R.D. Monte, P. Fornasiero, E. Fonda, J. Kaspar, M. Graziani, Journal of Catalysis 182 (1999) 378–389.
[23] J.R. McBride, K.C. Hass, B.D. Poindexter, W.H. Weber, Journal of Applied Physics 76 (1994) 2435–2441.
[24] E. Spanier, R.D. Robinson, F. Zhang, S.-W. Chan, I.P. Herman, Physical Review B 64 (2001) 245407.
[25] C. de Leitenburg, A. Trovarelli, J. Llorca, F. Cavani, G. Bini, Applied Catalysis A 139 (1996) 161–173.
[26] A. Trovarelli, F. Zamar, J. Llorca, C. de Leitenburg, G. Dolcetti, J.T. Kiss, Journal of Catalysis 169 (1997) 490–502.
[27] I. Kosacki, T. Suzuki, H.U. Anderson, P. Colomban, Solid State Ionics 149 (2002) 99–105.
[28] D. Andreeva, R. Nedyalkova, L. Ilieva, M.V. Abrashev, Applied Catalysis B 52 (2004) 157–165.
[29] F. Zhang, P. Wang, J. Koberstein, S. Khalid, S. Chan, Surface Science 563 (2004) 74–82.
[30] A. Galtayries, R. Sporken, J. Riga, G. Blanchard, R. Caudano, Journal of Electron Spectroscopy and Related Phenomena 88 (1998) 951–956.
[31] T.L. Barr, Journal of Physical Chemistry 82 (1978) 1801–1810.
[32] F.C. Meunier, D. Tibiletti, A. Goguet, D. Reid, R. Burch, Applied Catalysis A 289 (2005) 104.
[33] O. Pozdnyakova, D. Teschner, A. Wootsch, J. Kröhnert, B. Steinhauer, H. Sauer, L. Toth, F.C. Jentoft, A. Knop-Gericke, Z. Paál, R. Schlögl, Journal of Catalysis 237 (2006) 1–16.
[34] C. Binet, M. Daturi, J.-C. Lavalley, Catalysis Today 50 (1999) 207.
[35] F. Romero-Sarria, L.M. Martínez T., M.A. Centeno, J.A. Odriozola, Journal of Physical Chemistry C 111 (2007) 14469.
[36] K. Hanna, C. Carteret, Chemosphere 70 (2007) 178.
[37] J. Lichtenberger, M.D. Amiridis, Catalysis Today 98 (2004) 447.
[38] K.D. Dobson, A.J. McQuillan, Spectrochimica Acta, Part A 56 (2000) 557.